

Lesion Border Detection in Dermoscopy Images Using Ensembles of Thresholding Methods

M. Emre Celebi

Dept. of Computer Science
Louisiana State Univ., Shreveport, LA, USA
ecelebi@lsus.edu

Quan Wen

School of Computer Science and Engineering
Univ. of Electronic Science and Technology of China, Chengdu, P.R. China
quanwen@uestc.edu.cn

Sae Hwang

Dept. of Computer Science
Univ. of Illinois, Springfield, IL, USA
shwan2@uis.edu

Hitoshi Iyatomi

Dept. of Applied Informatics
Hosei Univ., Tokyo, Japan
iyatomi@hosei.ac.jp

Gerald Schaefer

Dept. of Computer Science
Loughborough Univ., Loughborough, UK
gerald.schaefer@ieee.org

December 31, 2013

Abstract

Dermoscopy is one of the major imaging modalities used in the diagnosis of melanoma and other pigmented skin lesions. Due to the difficulty and subjectivity of human interpretation, automated analysis of dermoscopy images has become an important research area. Border detection is often the first step in this analysis. In many cases, the lesion can be roughly separated from the background skin using a thresholding method applied to the blue channel. However, no single thresholding method appears to be robust enough to successfully handle the wide variety of dermoscopy images encountered in clinical practice. In this paper, we present an automated method for detecting lesion borders in dermoscopy images using ensembles of thresholding methods. Experiments on a difficult set of 90 images demonstrate that the proposed method is robust, fast, and accurate when compared to nine state-of-the-art methods.

1 Introduction

Invasive and in-situ malignant melanoma together comprise one of the most rapidly increasing cancers in the world. Invasive melanoma alone has an estimated incidence of 70,230 and an estimated total of 8,790 deaths in the United States in 2011 [1]. Early diagnosis is particularly important since melanoma can be cured with a simple excision if detected early.

Dermoscopy has become one of the most important tools in the diagnosis of melanoma and other pigmented skin lesions. This non-invasive skin imaging technique involves optical magnification and either liquid immersion and low angle-of-incidence lighting or cross-polarized lighting, making subsurface structures more easily visible when compared to conventional clinical images [2]. Dermoscopy allows the identification of dozens of morphological features such as pigment networks, dots/globules, streaks, blue-white areas, and blotches [3]. This reduces screening errors and provides greater differentiation between difficult lesions such as pigmented Spitz nevi and small, clinically equivocal lesions [4]. However, it has also been demonstrated that dermoscopy may actually lower the diagnostic accuracy in the hands of inexperienced dermatologists [5]. Therefore, in order to minimize the diagnostic errors that

result from the difficulty and subjectivity of visual interpretation, the development of computerized image analysis techniques is of paramount importance [6].

Automated border detection is often the first step in the automated or semi-automated analysis of dermoscopy images [7]. It is crucial for image analysis for two main reasons. First, the border structure provides important information for accurate diagnosis, as many clinical features, such as asymmetry, border irregularity, and abrupt border cutoff, are calculated directly from the border. Second, extraction of other important clinical features such as atypical pigment networks, globules, and blue-white areas, critically depends on the accuracy of border detection. Automated border detection is a challenging task due to several reasons: (i) low contrast between the lesion and the surrounding skin, (ii) irregular and fuzzy lesion borders, (iii) artifacts and intrinsic cutaneous features such as black frames, skin lines, blood vessels, hairs, and air bubbles, (iv) variegated coloring inside the lesion, and (v) fragmentation due to various reasons such as scar-like depigmentation.

Numerous methods have been developed for border detection in dermoscopy images [7]. Recent approaches include thresholding [8, 9], k-means clustering [10], fuzzy c-means clustering [11, 12], density-based clustering [13], meanshift clustering [14], gradient vector flow snakes [15, 16, 17], color quantization followed by spatial segmentation [18], statistical region merging [19], watershed transformation [20], dynamic programming [21, 22], and supervised learning [23, 24].

In this paper, we present a fast and accurate method for detecting lesion borders in dermoscopy images. The method involves the fusion several thresholding methods followed by various simple postprocessing steps. The rest of the paper is organized as follows. Section 2 describes the threshold fusion method and the postprocessing steps. Section 3 presents the experimental results. Finally, Section 4 gives the conclusions.

2 Threshold Fusion

In many dermoscopic images, the lesion can be roughly separated from the background skin using a thresholding method applied to the blue channel [7]. While there are a number of thresholding methods that perform well in general, the effectiveness of a method strongly depends on the statistical characteristics of the image [25]. Fig. 1 illustrates this phenomenon. Here, method 1(e) performs quite well. In contrast, methods 1(c), 1(d), and 1(f) underestimate the optimal threshold. Although method 1(f) is the most popular thresholding method in the literature [26], for this particular image, it performs the worst.

A possible approach to overcome this problem is to fuse the results provided by an ensemble of thresholding methods. In this way, it is possible to exploit the peculiarities of the participating thresholding methods synergistically, thus arriving at more robust final decisions than is possible with a single thresholding method. It should be noted that the goal of the fusion is not to outperform the individual thresholding methods, but to obtain accuracies comparable to that of the best thresholding method independently of the image characteristics. In this study, we adopted the threshold fusion method proposed by Melgani [25], which we describe briefly in the following.

Let $X = \{x_{mn} : m = 0, 1, \dots, M-1, n = 0, 1, \dots, N-1\}$ be the original scalar $M \times N$ image with L possible gray levels ($x_{mn} \in \{0, 1, \dots, L-1\}$) and $Y = \{y_{mn} : m = 0, 1, \dots, M-1, n = 0, 1, \dots, N-1\}$ be the binary output of the threshold fusion. Consider an ensemble of P thresholding methods. Let T_i and A_i ($i = 1, 2, \dots, P$) be the threshold value and the output binary image associated with the i -th method of the ensemble, respectively. Within a Markov Random Field (MRF) framework, the fusion problem can be formulated as an energy minimization task. Accordingly, the local energy function U_{mn} to be minimized for the pixel (m, n) can be written as follows:

$$U_{mn} = \beta_{SP} \cdot U_{SP} [y_{mn}, Y^S(m, n)] + \sum_{i=1}^P \beta_i \cdot U_{II} [y_{mn}, A_i^S(m, n)] \quad (1)$$

where S is a predefined neighborhood system associated with pixel (m, n) , $U_{SP}(\cdot)$ and $U_{II}(\cdot)$ refer to the spatial and inter-image energy functions, respectively, whereas β_{SP} and β_i ($i = 1, 2, \dots, P$) represent the spatial and inter-image parameters, respectively. The spatial energy function can be expressed as:

$$U_{SP} [y_{mn}, Y^S(m, n)] = - \sum_{y_{pq} \in Y^S(m, n)} I(y_{mn}, y_{pq}) \quad (2)$$

where $I(\cdot, \cdot)$ is the indicator function defined as:

$$I(y_{mn}, y_{pq}) = \begin{cases} 1 & \text{if } y_{mn} = y_{pq} \\ 0 & \text{otherwise} \end{cases} \quad (3)$$

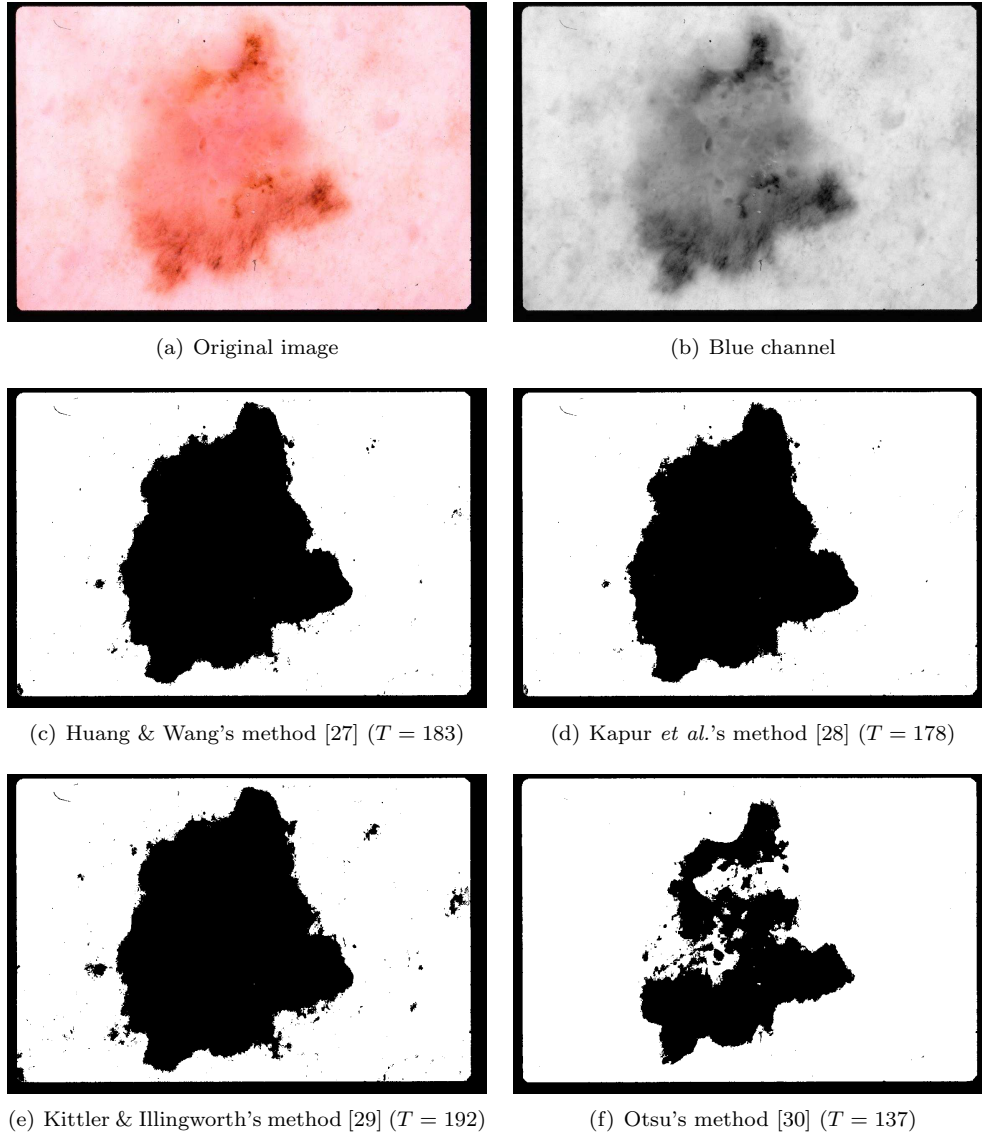


Figure 1: Comparison of various thresholding methods (T : threshold)

The inter-image energy function is defined as:

$$U_{II} [y_{mn}, A^S(m, n)] = - \sum_{A_i(p, q) \in A_i^S(m, n)} \alpha^i(x_{pq}) \cdot I[y_{mn}, A_i(p, q)] \quad (4)$$

where $\alpha^i(x_{mn}) = 1 - \exp(-\gamma |x_{mn} - T_i|)$ is a weight function.

This function controls the effect of unreliable decisions at the pixel level that can be incurred by the thresholding methods. At the global (image) level, decisions are weighed by the inter-image parameters β_i ($i = 1, 2, \dots, P$), which are computed as follows: $\beta_i = \exp(-\gamma |\bar{T} - T_i|)$ where \bar{T} is the average threshold value, i.e. $\bar{T} = (1/P) \sum_{i=1}^P T_i$.

The MRF fusion strategy proposed in [25] is as follows:

1. Apply each thresholding method of the ensemble to the image X to generate the set of thresholded images A_i ($i = 1, 2, \dots, P$).
2. Initialize Y by minimizing for each pixel (m, n) the local energy function U_{mn} defined in Eq. (1) without the spatial energy term, i.e. by setting $\beta_{SP} = 0$.
3. Update Y by minimizing for each pixel (m, n) the local energy function U_{mn} defined in Eq. (1) including the spatial energy term, i.e. by setting $\beta_{SP} \neq 0$.

4. Repeat step (3) K_{max} times or until the number of different labels in Y computed over the last two iterations becomes very small.

In our preliminary experiments, we observed that, besides being computationally demanding, the iterative part (step 3) of the fusion method makes only marginal contribution to the quality of the results. Therefore, in this study, we considered only the first two steps. The γ parameter was set to the recommended value of 0.1 [25]. For computational reasons, α and β values were precalculated and the neighborhood system S was chosen as a 3×3 square. We considered four popular thresholding methods to construct the ensemble: Huang & Wang’s fuzzy similarity method [27], Kapur *et al.*’s maximum entropy method [28], Kittler & Illingworth’s minimum error thresholding method [29], and Otsu’s clustering based method [30].

After performing the threshold fusion on the blue channel, the final border was obtained by filling the binary fusion output and removing all but the largest (4-)connected component in it. Fig. 2 shows the fusion result for the image given in Fig. 1(a). Here the fusion output is delineated in red, whereas the manual border (see Section 3) is delineated in blue. It can be seen that the former is mostly contained inside the latter. This was observed in many cases because the automated methods tend to find the sharpest pigment change, whereas the dermatologists choose the outmost detectable pigment [7]. The discrepancy between the two borders can be reduced by expanding the fusion output using morphological dilation. A circular structuring element with a radius of $R = \lfloor kD/512 \rfloor$, where $\lfloor \cdot \rfloor$ and D denote the floor operation and diameter of the lesion object in the fusion output, respectively and k is a scaling factor, which in this study was set to $k = 7$. It can be seen that after the expansion, the fusion output (delineated in green) is significantly closer to the manual border, which is also reflected by a reduction in the XOR error (see Section 3) from 17.14% to 8.79%.

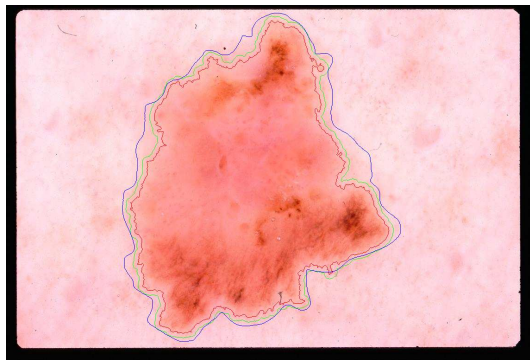


Figure 2: Fusion result for Fig. 1(a)

3 Experimental Results and Discussion

The proposed border detection method was tested on a set of 90 dermoscopy images (23 invasive malignant melanoma and 67 benign) obtained from the EDRA Interactive Atlas of Dermoscopy [2], and three private dermatology practices [19]. An experienced dermatologist determined the manual borders by selecting a number of points on the lesion border, which were then connected by a second-order B-spline. The presented fusion method was compared to nine recent methods using the XOR measure [31] given by $\varepsilon = \text{Area}(AB \oplus MB) / \text{Area}(MB)$, where AB is the binary output of an automated method, MB is the binary border drawn by the dermatologist, \oplus is the exclusive-OR operation that determines the pixels for which the AB and MB disagree, and $\text{Area}(I)$ denotes the number of pixels in the binary image I .

Table 1 gives the mean (μ) and standard deviation (σ) percent XOR errors for the ten automated methods. It can be seen that the presented fusion method is significantly more accurate when compared to the other methods. Furthermore, our method is more stable as evidenced by its low standard deviation.

Table 2 shows the statistics for the individual thresholding methods. Note that, the outputs of these methods were postprocessed as described in Section 2. It can be seen that the individual methods obtain significantly higher mean errors when compared to the fusion method. This is because, as explained in Section 2, the individual methods are more prone to catastrophic failures when given pathological input images. The high standard deviation values also support this explanation. Only the performance of Otsu’s method is close to the performance of the fusion. However, as mentioned earlier, the goal of fusion is not to outperform the individual thresholding methods, but to obtain results comparable to that of the best thresholding method independently of the image characteristics.

Table 1: Error statistics for the border detection methods

Method	Benign		Melanoma		All	
	μ	σ	μ	σ	μ	σ
[11]	22.99	12.61	28.31	15.25	24.35	13.45
[15]	13.69	5.59	19.34	9.33	15.13	7.13
[8]	10.51	4.73	11.85	6.00	10.86	5.08
[14]	11.53	9.74	13.29	7.42	11.98	9.19
[18]	10.83	6.36	13.75	7.59	11.58	6.77
[19]	11.38	6.23	10.29	5.84	11.11	6.12
[10]	21.56	25.19	23.51	16.06	22.06	23.13
[9]	12.95	6.17	16.93	7.16	13.96	6.63
[23]	10.07	4.34	18.17	26.96	12.14	14.36
<i>Fusion</i>	8.36	4.33	8.17	3.13	8.31	4.06

Table 2: Error statistics for the individual thresholding methods

Method	Benign		Melanoma		All	
	μ	σ	μ	σ	μ	σ
Huang & Wang	9.01	5.43	15.65	29.82	10.70	15.82
Kapur <i>et al.</i>	20.99	18.20	14.88	14.21	19.43	17.40
Kittler & Illingworth	10.08	8.08	21.34	38.17	12.95	20.81
Otsu	8.66	4.93	10.64	5.81	9.16	5.21

Fig. 3 shows sample border detection results obtained by the proposed method. It can be seen that the method performs well even in the presence of complicating factors such as diffuse edges, blood vessels, and skin lines.

4 Conclusions

In this paper, an automated threshold fusion method for detecting lesion borders in dermoscopy images was presented. Experiments on a difficult set of images demonstrated that this method compares favorably to nine recent border detection methods. In addition, the method is easy to implement, extremely fast (0.1 seconds for a typical image of size 768×512 pixels on an Intel QX9300 2.53GHz computer) and it does not require sophisticated postprocessing.

The presented method may not perform well on images with significant amount of hair or bubbles since these elements alter the histogram, which in turn results in biased threshold computations. For images with hair, a preprocessor such as *DullRazorTM* [32] might be helpful. Unfortunately, the development of a reliable bubble removal method remains an open problem.

Acknowledgments

This publication was made possible by grants from the Louisiana Board of Regents (LEQSF2008-11-RD-A-12), US National Science Foundation (0959583, 1117457), and National Natural Science Foundation of China (61050110449, 61073120).

References

- [1] R. Siegel, E. Ward, O. Brawley, and A. Jemal, “Cancer Statistics, 2011,” *CA: A Cancer Journal for Clinicians*, vol. 61, no. 4, pp. 212–236, 2011.
- [2] G. Argenziano, H.P. Soyer, and V. De Giorgi *et al.*, *Dermoscopy: A Tutorial*, EDRA Medical Publishing & New Media, 2002.
- [3] S. Menzies, K. Crotty, C. Ingvar, and W. McCarthy, *Dermoscopy: An Atlas*, McGraw-Hill, 3rd edition, 2009.

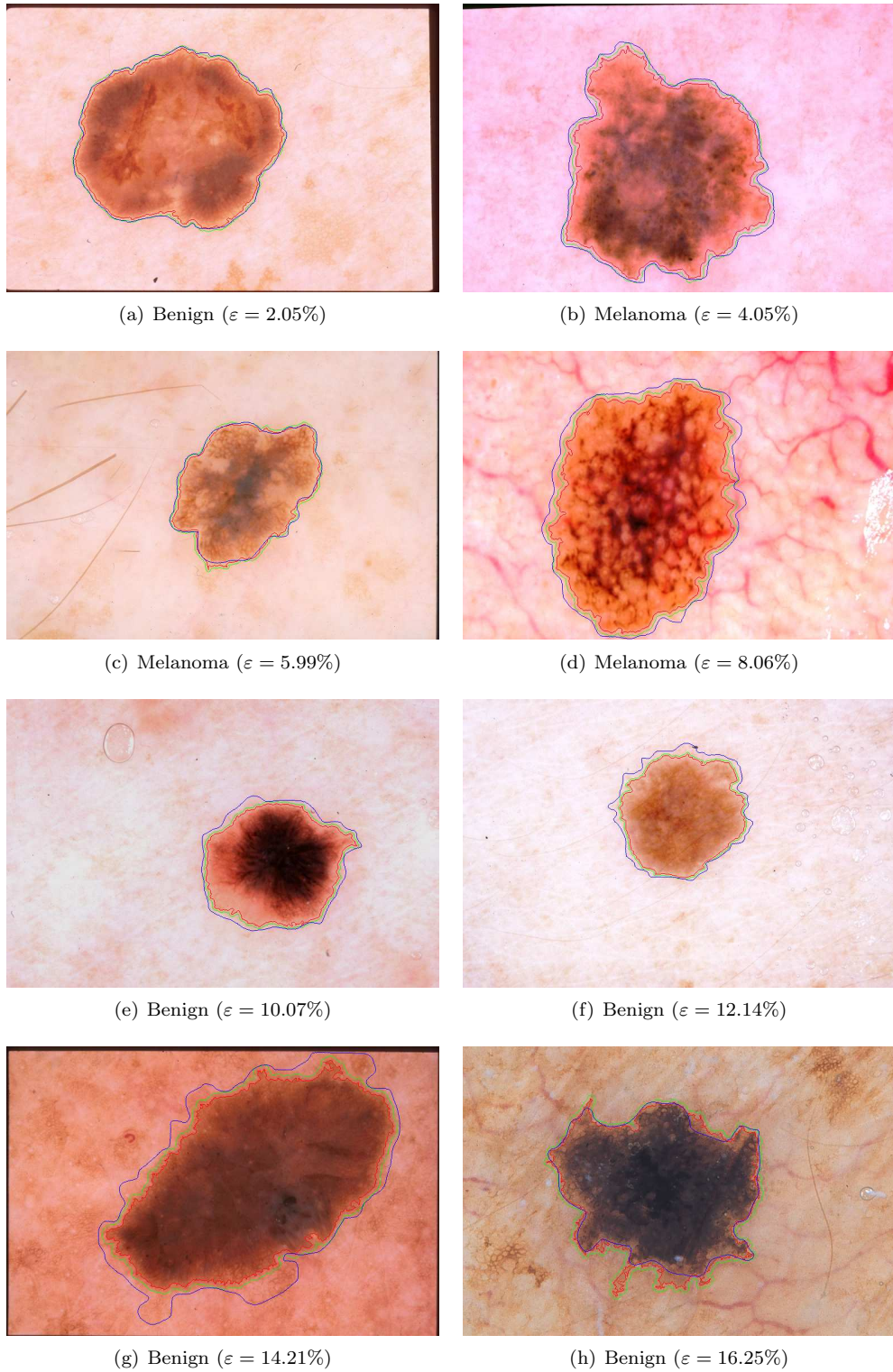


Figure 3: Sample border detection results

- [4] K. Steiner, M. Binder, M. Schemper, K. Wolff, and H. Pehamberger, “Statistical Evaluation of Epiluminescence Microscopy Criteria for Melanocytic Pigmented Skin Lesions,” *Journal of the American Academy of Dermatology*, vol. 29, no. 4, pp. 581–588, 1993.
- [5] M. Binder, M. Schwarz, A. Winkler, A. Steiner, A. Kaider, K. Wolff, and H. Pehamberger, “Epiluminescence

- Microscopy. A Useful Tool for the Diagnosis of Pigmented Skin Lesions for Formally Trained Dermatologists,” *Archives of Dermatology*, vol. 131, no. 3, pp. 286–291, 1995.
- [6] M. E. Celebi, H. A. Kingravi, B. Uddin, H. Iyatomi, A. Aslandogan, W. V. Stoecker, and R. H. Moss, “A Methodological Approach to the Classification of Dermoscopy Images,” *Computerized Medical Imaging and Graphics*, vol. 31, no. 6, pp. 362–373, 2007.
- [7] M. E. Celebi, H. Iyatomi, G. Schaefer, and W. V. Stoecker, “Lesion Border Detection in Dermoscopy Images,” *Computerized Medical Imaging and Graphics*, vol. 33, no. 2, pp. 148–153, 2009.
- [8] H. Iyatomi, H. Oka, M. E. Celebi, M. Hashimoto, M. Hagiwara, M. Tanaka, and K. Ogawa, “An Improved Internet-based Melanoma Screening System with Dermatologist-like Tumor Area Extraction Algorithm,” *Computerized Medical Imaging and Graphics*, vol. 32, no. 7, pp. 566–579, 2008.
- [9] R. Garnavi, M. Aldeen, M. E. Celebi, G. Varigos, and S. Finch, “Border Detection in Dermoscopy Images Using Hybrid Thresholding on Optimized Color Channels,” *Computerized Medical Imaging and Graphics*, vol. 35, no. 2, pp. 105–115, 2011.
- [10] H. Zhou, M. Chen, L. Zou, R. Gass, L. Ferris, L. Drogowski, and J. M. Rehg, “Spatially Constrained Segmentation of Dermoscopy Images,” in *Proceedings of the 5th IEEE International Symposium on Biomedical Imaging*, 2008, pp. 800–803.
- [11] P. Schmid, “Segmentation of Digitized Dermatoscopic Images by Two-Dimensional Color Clustering,” *IEEE Transactions on Medical Imaging*, vol. 18, no. 2, pp. 164–171, 1999.
- [12] H. Zhou, G. Schaefer, A. Sadka, and M. E. Celebi, “Anisotropic Mean Shift Based Fuzzy C-Means Segmentation of Dermoscopy Images,” *IEEE Journal of Selected Topics in Signal Processing*, vol. 3, no. 1, pp. 26–34, 2009.
- [13] M. Mete, S. Kockara, and K. Aydin, “Fast Density-Based Lesion Detection in Dermoscopy Images,” *Computerized Medical Imaging and Graphics*, vol. 35, no. 2, pp. 128–136, 2011.
- [14] R. Melli, C. Grana, and R. Cucchiara, “Comparison of Color Clustering Algorithms for Segmentation of Dermatological Images,” in *Proceedings of the SPIE Medical Imaging Conference*, 2006, pp. 1211–1219.
- [15] B. Erkol, R. H. Moss, R. J. Stanley, W. V. Stoecker, and E. Hvatum, “Automatic Lesion Boundary Detection in Dermoscopy Images Using Gradient Vector Flow Snakes,” *Skin Research and Technology*, vol. 11, no. 1, pp. 17–26, 2005.
- [16] H. Zhou, G. Schaefer, M. E. Celebi, F. Lin, and T. Liu, “Gradient Vector Flow with Mean Shift for Skin Lesion Segmentation,” *Computerized Medical Imaging and Graphics*, vol. 35, no. 2, pp. 121–127, 2011.
- [17] Q. Abbas, M. E. Celebi, and I. F. Garcia, “A Novel Perceptually-Oriented Approach for Skin Tumor Segmentation,” *International Journal of Innovative Computing, Information and Control*, vol. 8, no. 3, pp. 1837–1848, 2012.
- [18] M. E. Celebi, Y. A. Aslandogan, W. V. Stoecker, H. Iyatomi, H. Oka, and X. Chen, “Unsupervised Border Detection in Dermoscopy Images,” *Skin Research and Technology*, vol. 13, no. 4, pp. 454–462, 2007.
- [19] M. E. Celebi, H. A. Kingravi, H. Iyatomi, A. Aslandogan, W. V. Stoecker, R. H. Moss, J. M. Malters, J. M. Grichnik, A. A. Marghoob, H. S. Rabinovitz, and S. W. Menzies, “Border Detection in Dermoscopy Images Using Statistical Region Merging,” *Skin Research and Technology*, vol. 14, no. 3, pp. 347–353, 2008.
- [20] H. Wang, R. H. Moss, X. Chen, R. J. Stanley, W. V. Stoecker, M. E. Celebi, J. M. Malters, J. M. Grichnik, A. A. Marghoob, H. S. Rabinovitz, S. W. Menzies, and T. M. Szalapski, “Modified Watershed Technique and Post-Processing for Segmentation of Skin Lesions in Dermoscopy Images,” *Computerized Medical Imaging and Graphics*, vol. 35, no. 2, pp. 116–120, 2011.
- [21] Q. Abbas, M. E. Celebi, I. F. Garcia, and M. Rashid, “Lesion Border Detection in Dermoscopy Images Using Dynamic Programming,” *Skin Research and Technology*, vol. 17, no. 1, pp. 91–100, 2011.
- [22] Q. Abbas, M. E. Celebi, and I. F. Garcia, “Skin Tumor Area Extraction Using an Improved Dynamic Programming Approach,” *Skin Research and Technology*, vol. 18, no. 2, pp. 133–142, 2012.

- [23] G. Schaefer, M. I. Rajab, M. E. Celebi, and H. Iyatomi, “Colour and Contrast Enhancement for Improved Skin Lesion Segmentation,” *Computerized Medical Imaging and Graphics*, vol. 35, no. 2, pp. 99–104, 2011.
- [24] P. Wighton, T. K. Lee, H. Lui, D. I. McLean, and M. S. Atkins, “Generalizing Common Tasks in Automated Skin Lesion Diagnosis,” *IEEE Transactions on Information Technology in Biomedicine*, vol. 15, no. 4, pp. 622–629, 2011.
- [25] F. Melgani, “Robust Image Binarization with Ensembles of Thresholding Algorithms,” *Journal of Electronic Imaging*, vol. 15, pp. 023010, 2006.
- [26] M. Sezgin and B. Sankur, “Survey over Image Thresholding Techniques and Quantitative Performance Evaluation,” *Journal of Electronic Imaging*, vol. 13, pp. 146–165, 2004.
- [27] L.-K. Huang and M.-J. J. Wang, “Image Thresholding by Minimizing the Measures of Fuzziness,” *Pattern Recognition*, vol. 28, no. 1, pp. 41–51, 1995.
- [28] J. N. Kapur, P. K. Sahoo, and A. K. C. Wong, “A New Method for Gray-Level Picture Thresholding Using the Entropy of the Histogram,” *Computer Vision, Graphics, and Image Processing*, vol. 29, no. 3, pp. 273–285, 1985.
- [29] J. Kittler and J. Illingworth, “Minimum Error Thresholding,” *Pattern Recognition*, vol. 19, no. 1, pp. 41–47, 1986.
- [30] N. Otsu, “A Threshold Selection Method from Gray Level Histograms,” *IEEE Transactions on Systems, Man and Cybernetics*, vol. 9, no. 1, pp. 62–66, 1979.
- [31] G. A. Hance, S. E. Umbaugh, R. H. Moss, and W. V. Stoecker, “Unsupervised Color Image Segmentation with Application to Skin Tumor Borders,” *IEEE Engineering in Medicine and Biology Magazine*, vol. 15, no. 1, pp. 104–111, 1996.
- [32] T. K. Lee, V. Ng, R. Gallagher, A. Coldman, and D. McLean, “DullRazor: A Software Approach to Hair Removal from Images,” *Computers in Biology and Medicine*, vol. 27, no. 6, pp. 533–543, 1997.